HOSTED BY
ELSEVIER

Available online at www.sciencedirect.com

ScienceDirect

journal homepage: http://ees.elsevier.com/ejbas/default.asp

Egyptian Journal of Basic and Applied Sciences

Full Length Article

Temperature dependent current–voltage and photovoltaic properties of chemically prepared (p)Si/(n)Bi_2S_3 heterojunction

Amir Hussain *

Department of Physics, Gauhati University, Guwahati, Assam 781014, India

ARTICLE INFO

Article history:
Received 4 October 2015
Received in revised form 18 June 2016
Accepted 21 June 2016
Available online 1 July 2016

Keywords:
Nanocrystalline
Heterojunction
Silicon
Series resistance
Photovoltaic

ABSTRACT

Ni-doped nanocrystalline Bi_2S_3 thin film is deposited on boron doped single crystal (p)-Si substrate by chemical bath deposition to form (p)Si/(n)Bi_2S_3 heterojunction structure. The electrical characterization of the (p)Si/(n)Bi_2S_3 heterojunction is carried out in the temperature range of 300 K–340 K and capacitance–voltage characteristics is measured at a frequency of 1 KHz at 300 K. Various junction parameters are calculated from the I–V characteristics. The ideality factor is found to be greater than unity with high series resistance. The ideality factor and series resistance decreases, whereas the saturation current density increases with increase in temperature. The *J*–V characteristics under illumination showed poor photovoltaic effect of the junction. The existence of higher value of ideality factor and large number of interface states in (p)Si/(n) Bi_2S_3 heterojunction reduced the photovoltaic conversion efficiency.

1. Introduction

Bismuth Sulphide is a member of V–VI semiconductor compounds whose band gap energy 1.7 eV lies in the visible range of the solar energy spectrum, which makes it very useful for solar energy conversion devices [1–3]. Bohr exciton radius of bulk Bi_2S_3 is 28.9 nm [4], which implies that significant quantum confinement effect can be observed at relatively large Bi_2S_3 nanoparticles. Bi_2S_3 is one of the earliest materials known to exhibit photoconducting properties [5]. Due to its significant thermoelectric effect, this material is important in view of its thermoelectric application as well [6]. It is widely used in optoelectronics, photoelectrochemical devices, thermoelectric cooler, electrical switching, solar selective coatings, and decorative coatings [5,7]. Nanostructures of Bi_2S_3 have potential applications in electrochemical hydrogen storage, hydrogen sensors, X-ray computed tomography imaging, biomolecule detection and photoresponsive materials [8].

Much research have been carried out on the preparation, characterization and applications of Bi_2S_3 thin films by employing several deposition techniques such as chemical deposition [9–16], vacuum evaporation [17–20], cathodic electrodeposition [21], anodic electrodeposition [22], hot-wall method [23], solution gas interface [24], spray deposition [7,25–28], ultrasonic methods [29,30], microwave irradiation [31,32],

* *E-mail address:* hussainmakak@gmail.com.
http://dx.doi.org/10.1016/j.ejbas.2016.06.003

hydrothermal synthesis [33–35], and solvothermal decomposition [36] etc.

There are limited literature pertaining to the preparation and characterization of heterojunctions based on Bi_2S_3. Pineda et al. [37] fabricated hybrid solar cells of the configuration ITO/Bi_2S_3/P3OT/Au [(P3OT) is poly3-octylthiophene polymer]. They investigated the photovoltaic performance of the solar cell and reported that the cell using a Bi_2S_3 film of thickness 50 nm had the highest open-circuit voltage of 440 mV and short-circuit current density of 0.022 mA/cm^2. Recently, Martinez et al. [38] fabricated hybrid heterojunctions by using Bi_2S_3, NCs and P3HT poly (3-hexylthiophene) polymer with a power conversion efficiency of 1%. Becerra et al. [39] have analysed the feasibility of combining p-Si with an n-Bi_2S_3 thin film to form thin film solar cell using evaporated (n)Bi_2S_3 on (p)Si. They reported short-circuit current density of 3 mA/cm^2, open-circuit voltage of 360 mV, and efficiency of 0.5%, which improved to 7.2 mA/cm^2, 485 mV and 1.7%, respectively, after heating the cell in forming gas. Moreno-Garcia et al. [40] have fabricated (n)Bi_2S_3/(p)PbS solar cell by chemical CBD method. They carried out an extensive study to explore the relevance of each thin film component and suggested ways to improve the cell parameters. Their best (n)Bi_2S_3/(p)PbS solar cell junctions produced open-circuit voltage of 280 mV and short-circuit current density of 6 mA/cm^2 and energy conversion efficiency of 0.5%. The same research group [41] extended their work on (n)Bi_2S_3/(p)PbS solar cells by introducing CdS and ZnS window layers in their solar cell structure and reported an improvement of the various junction parameters. Kachari et al. [42] reported the fabrication of Al/(p)Bi_2S_3 Schottky barrier junction by vacuum evaporation method. They have evaluated the various junction parameters from the I–V characteristics of the junction. Further, they investigated the photovoltaic performance of the junction. Bao et al. [43] reported the formation of Schottky contact between Bi_2S_3 nanowires and gold (Au) electrode. The photo-switchable conductivity of individual Bi_2S_3 nanowires was studied, indicating possible applications in optoelectronic nano-devices. Bessekhouad et al. [44] prepared (n)Bi_2S_3/(n)TiO_2 heterojunctions by direct mixture of both constituents and by precipitation of the Bi_2S_3 with commercial TiO_2 at different concentrations. They have analysed (n)Bi_2S_3/(n)TiO_2 junction by UV-Vis spectroscopy and established that the junctions were able to absorb the light up to 800 nm. Moreno-García et al. [45] fabricated CdS/(n)Bi_2S_3/(p)PbS solar cell and reported open-circuit voltage of 250 mV and short-circuit current density of 3.45 mA/cm^2. Bi_2S_3 film was introduced basically to secure stability for the CdS/ PbS junction. Wang et al. [46] synthesized Bi_2S_3 nanorods and nanowires. Further they fabricated bulk hybrid heterojunction solar cells by blending the Bi_2S_3 nanorods or nanowires with MDMO-PPV polymer (poly [2-methoxy-5-(3′,7′-dimethyloctyloxy)-1,4-phenylenevinylene]). Ladhe et al. [47] have chemically prepared (n)Bi_2S_3 and (p)CuSCN layers to fabricate (n)Bi_2S_3/(p)CuSCN heterojunction on fluorine doped tin oxide (FTO) coated glass substrates. They successfully employed the heterojunction as a Liquefied Petroleum Gas (LPG) sensor at room temperature. Rath et al. [48] reported the first solution-processed heterojunction solar cells based on p-type PbS quantum dots and n-type Bi_2S_3 nanocrystals. In this solar cell nanostructured n-type Bi_2S_3 was used as electron acceptor. They reported a power conversion efficiency of 1.6% for 860 nm PbS QDs and over 1% for 1300 nm PbS QDs.

2. Preparation of (p)Si/(n)Bi_2S_3 heterojunction

The (p)Si/(n)Bi_2S_3 heterojunctions are prepared by depositing 1.5 wt% Ni-doped Bi_2S_3 thin films on boron doped p-type silicon wafer by chemical bath deposition technique. The silicon wafers use for the fabrication of the heterojunction structure is mirror like p-type (100) orientation with resistivity 1–10 Ωcm and 350 ± 25 μm thickness. For the deposition of Ni-doped Bi_2S_3 film on silicon wafer, 5 ml of 0.5 M $Bi(NO_3)_3$ dissolved in 2 ml of Tri-ethanolamine (TEA) and 4 ml of 1 M $CH_3CS.NH_2$ are mixed together and 1.wt% of $Ni(NO_3)_3$ as Ni^{3+} sources is added to the resultant solution. The resultant solution is stirred for 20 min at room temperature to get uniform mixture solution. Finally, 39 ml of distilled water is added to the resultant solution to obtain a total volume of 50 ml. The silicon substrates are immersed vertically into the solution supported by the wall of the beaker and heated at 318 K for 20 min. The resultant solution changes from brown to dark brown colour, which indicates the initiation of Bi_2S_3 film formation. The solution is kept at room temperature for 2 h for further deposition. After deposition, the Si substrates coated with nanocrystalline Ni-doped Bi_2S_3 film are taken out and washed with distilled water and dried in open air. The films deposited on the polished surface of the Si substrates are removed with the help of dilute nitric acid and again washed with distilled water. Thickness of the Bi_2S_3 film deposited on the Si substrate is measured by Tolansky method as discussed in our earlier published paper [49]. The aluminium 'Al' electrodes are deposited onto the back surface of silicon wafers by vacuum evaporation for ohmic contact. The metal aluminium 'Al' electrodes, which acts as upper electrodes, are vacuum deposited on the Bi_2S_3 thin film through a suitable mask for ohmic contact to form the structure Al/(p)Si/(n) Bi_2S_3/Al as shown in Fig. 1. Thus, nine heterojunctions each of equal area of 0.04 cm^2 are obtained. Surface morphology of the film deposited on the Si substrate is studied using JEOL-JSM 6360 operating at 20 kV. Keithley

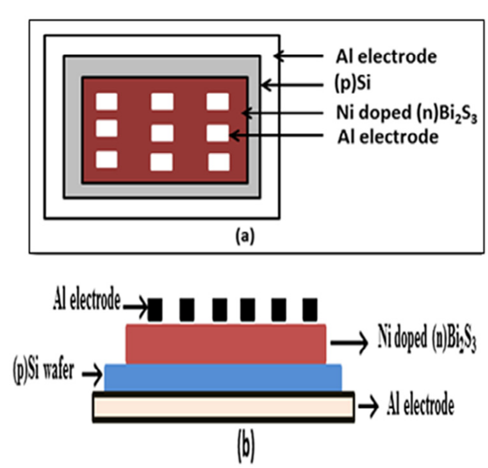

Fig. 1 – Schematic diagram of Al/(p)Si/(n)Bi_2S_3/Al structure: (a) view from above, (b) lateral view.

Table 1 – Details of a typical (p)Si/(n)Bi_2S_3 junction preparation.

Thickness of the (p)Si wafer (μm)	Thickness of (n) Bi_2S_3 (nm)	Concentration (N_a) $10^{16}/cm^3$	Concentration (N_d) $10^{16}/cm^3$
350 ± 25	228	5.6	2.622

Electrometer (6514) and Rishabh multimeter (14S) are used for measuring I–V characteristics of the (p)Si/(n)Bi2S3 heterojunction and C–V characteristics by using Systronics LCR-Q meter (928). The film deposited on the Si substrate is found to be n-type as determined by the hot probe method. The temperature on the sample surface is measured by Instron (In-303) digital temperature controller using PT-100 sensor. For forward bias, the positive and negative terminals of the voltage source are connected to upper and lower 'Al' electrodes. The details of the sample prepared are given in Table 1.

3. Results and discussions

3.1. *Reaction mechanism*

The deposition process of Bi_2S_3 film is based on the slow release of Bi^{3+} and S^{2-} ions in the solution, which then condense ion by ion or cluster by cluster on the surface of the boron doped p-Si substrate. The concentration of Bi^{3+} and S^{2-} ions in the solution controls the rate of Bi_2S_3 formation. The rate of Bi^{3+} ions is controlled by TEA, which forms a complex $Bi[(TEA)n]^{3+}$ with Bi^{3+}. Ni-doped Bi_2S_3 films are prepared by adding 1.5 wt% of nickel nitrate $Ni(NO_3)_2$ to the following procedure and the reaction mechanism are given as

$$Bi(NO_3)_3.5H_2O + TEA \rightarrow [Bi(TEA)]^{+3} + 5H_2O + NO_3^- \quad (1)$$

$$[Bi(TEA)]^{+3} \rightarrow Bi^{+3} + TEA \quad (2)$$

$$CH_3CSNH_2 + OH^- \rightarrow CH_3CONH_2 + SH^- \quad (3)$$

$$SH^- + OH^- \rightarrow S^{-2} + H_2O \quad (4)$$

$$Ni(NO_3)_2 \rightarrow Ni^{+2} + NO_3^- \quad (5)$$

Then the overall chemical reaction is as follows

$$Bi^{3+} + Ni^{2+} + S^{2-} \rightarrow Bi_{2-x}Ni_xS_3 \quad (6)$$

3.2. *Surface morphology studies*

The surface morphology of the Ni-doped Bi_2S_3 film deposited on the silicon substrate has been investigated by scanning electron microscope (SEM) operating with an accelerating voltage 20 kV as shown in Fig. 2. It is seen that the surface is well covered without any void or pin hole with irregularly shaped grains of random size. These irregularly shaped grains of random size are interconnected with each other to form a cluster. Agglomeration of small crystallites in the film is also evident from the photograph. Such agglomeration makes it difficult to evaluate the grain size from SEM image. It is also clear from this image that there is a common characteristic of the grains in their spherical shape.

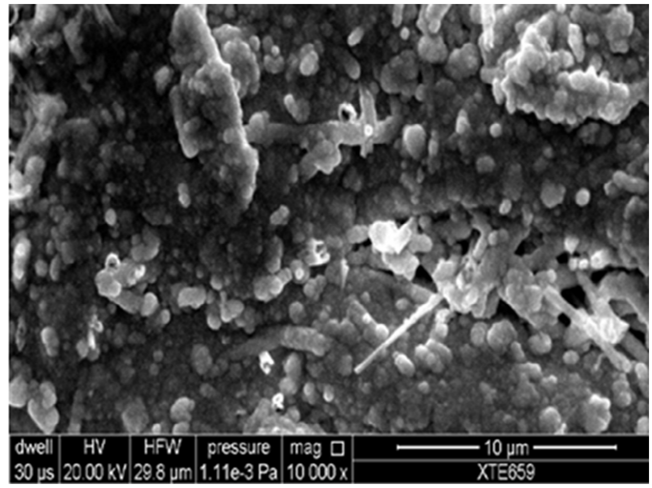

Fig. 2 – SEM photographs of nanoparticles Bi_2S_3.

3.3. *Current–voltage characteristics of (p)Si/(n)Bi_2S_3 heterojunctions*

The current–voltage characteristics of a typical (p)Si/(n)Bi_2S_3 junction in dark and under illumination (1100 Lux) are shown in Fig. 3. The junction is found to exhibit rectifying characteristics with small reverse current, indicating the existence of a barrier between the Si wafer and Bi_2S_3 film. The temperature dependence of the current–voltage characteristics of the prepared junction has been studied in the dark within temperature range from 300 K to 340 K. The temperature dependence of current–voltage characteristics for forward bias has been shown in Fig. 4. At higher bias voltage, the current

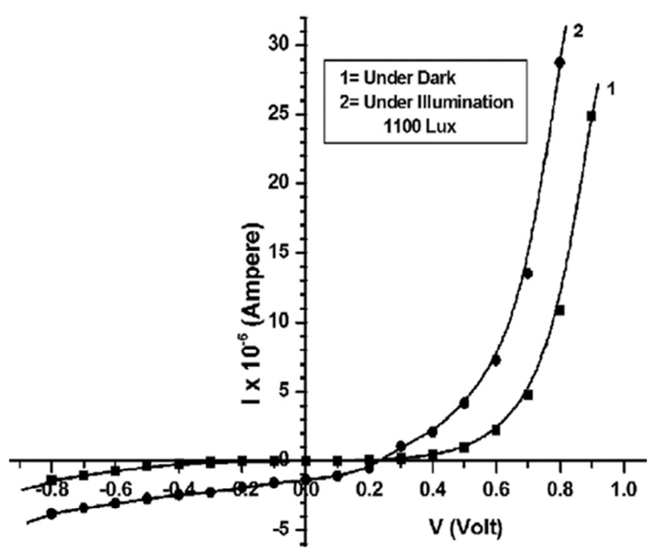

Fig. 3 – I–V characteristics of a typical (p)Si/(n)Bi_2S_3 junction in the dark and under illumination.

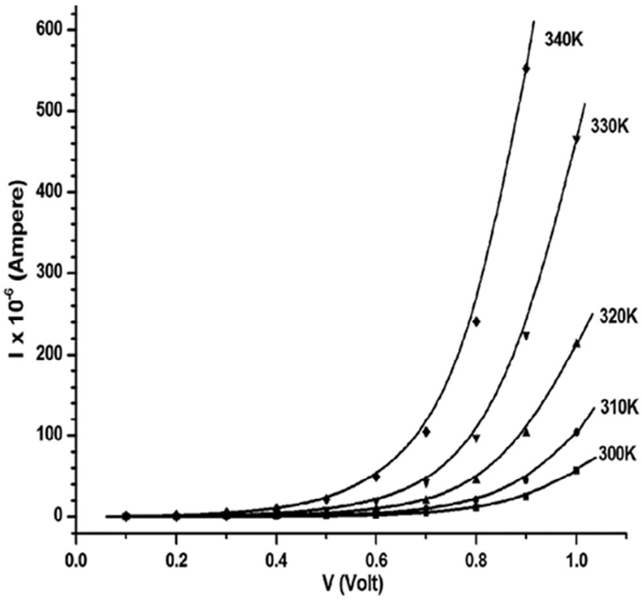

Fig. 4 – I–V characteristics of a typical (p)Si/(n)Bi_2S_3 heterojunction at different temperatures in the dark.

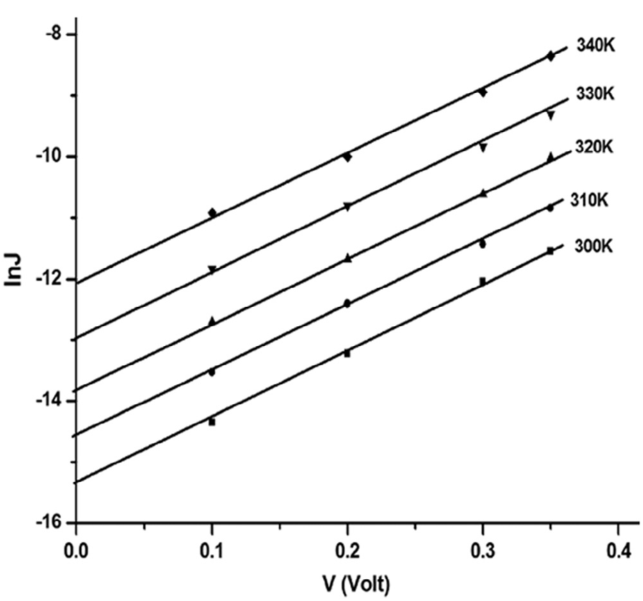

Fig. 5 – ln J vs V plot of a typical (p)Si/(n)Bi_2S_3 heterojunction.

has been observed to increase more rapidly as the temperature is increased. At low temperature, the carriers do not have sufficient energy to surmount the high barrier but they are able to surmount the lower barriers. Consequently, current will flow through patches of the lower Schottky barrier height [50]. With raising temperature, more and more electrons have enough energy to cross the higher barrier. As a result, the current transport is dominated by the current that flows over the higher barrier. Therefore the dominant barrier height increases with temperature [51].

Fig. 5 shows lnJ vs V plots for a typical (p)Si/(n)Bi_2S_3 heterojunction in the dark at different temperatures. The straight fitting of lnJ vs V shows that current, carrying mechanism over the heterojunction barrier, is dominated by the thermionic mechanism, current density–voltage relation is given by the relation [52]

$$J = J_s \exp\left[\frac{qV}{nkT}\right] \tag{7}$$

where V is the applied voltage and J_s is the saturation current density given as

$$J_s = \frac{qA^*TV_{bi}}{k}\exp\left(-\frac{qV_{bi}}{kT}\right) \tag{8}$$

where A^* is the Richardson constant, V_{bi} is the built-in potential, k is the Boltzmann's constant and T is the temperature.

The ideality factors (n) and saturation current density (J_s) are calculated from the slopes and intercepts of these plots respectively. The estimated values of diode ideality factors and saturation current densities at different temperatures of the typical (p)Si/(n)Bi_2S_3 heterojunction are given in Table 2. The saturation current density J_s and ideality factor (n) are dependent on temperature. The greater value of ideality factor than unity is attributed to factors such as presence of interfacial layer, image force lowering of built-in potential, recombination of electrons and holes in depletion region, tunnelling effect and barrier height inhomogeneity [53–55].

From the measured values of J_s at different temperatures, a plot of $\ln(J_s/T)$ versus T^{-1} has been drawn as shown in Fig. 6. The plot is almost a straight line, which indicates that the current transport process follows the relation (7) as discussed above. From the slope of the plot, the built-in potential V_{bi} of the junction is calculated and values are given in Table 2. The ideality factor 'n' and saturation current density 'J_s' of the junction at different temperatures are estimated from the slopes and intercepts of lnJ vs V plot (Fig. 5) respectively. The calculated values are tabulated in Table 2. From the estimated values

Table 2 – Junction parameters of a typical (P)Si/(n)Bi_2S_3 heterojunction.

Temperature (K)	Ideality factor (n)	Saturation current density J_s (10^{-6} Acm-2)	Built-in potential (from C–V) V_{bi} (eV)	Built-in potential (from I–V) V_{bi} (eV)	Series resistance (Ω)
					Dark
300	3.6	0.22	0.69	0.66	2447
310	3.5	0.47			932
320	3.4	0.98			446
330	3.3	2.34			260
340	3.2	5.69			83

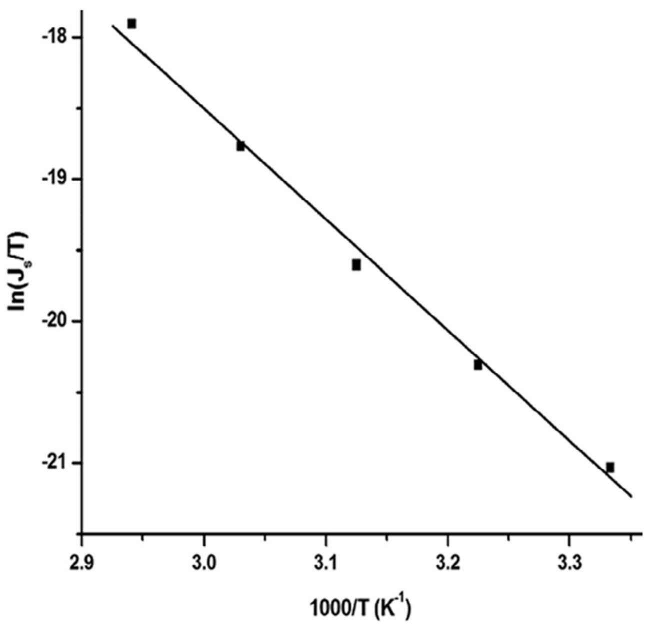

Fig. 6 – ln (J_s/T) versus T^{-1} plots of a typical (p)Si/(n)Bi_2S_3 heterojunction.

of J_s for different temperatures, lnJ_s/T vs T^{-1} graph is plotted for the junction as shown in Fig. 6. The built-in potential V_{bi} of the junction is calculated from the slope of the plot and the value is given in Table 2.

3.4. *Effect of series resistance on I–V characteristics of the (p)Si/(n)Bi_2S_3 heterojunction*

As depicted in Fig. 7 for higher voltages, the lnI vs V plots of the junctions have been observed to deviate from linearity. This deviation gives an indication of the presence of series resistance R_s associated with the neutral region of the junction. The series resistance are estimated from I vs ΔV plots of the junction. Fig. 8 represents the I vs ΔV plots of a typical (p)Si/(n)Bi_2S_3 junction at 300 K in the dark, where ΔV is the voltage due to series resistance. The value of R_s of a typical (p)Si/(n)Bi_2S_3 junction at different temperatures are found to be in the range 2447–83 Ω as given in Table 2. The series resistance of the (p)Si/(n)Bi_2S_3 junction is found to decrease with an increase in temperature. With increasing temperature, the number of free charge carriers is also increased due to either their bond breaking or by the de-trapping mechanism [56]. As a result, the series resistance of the (p)Si/(n)Bi_2S_3 junction decreases with an increase in temperature.

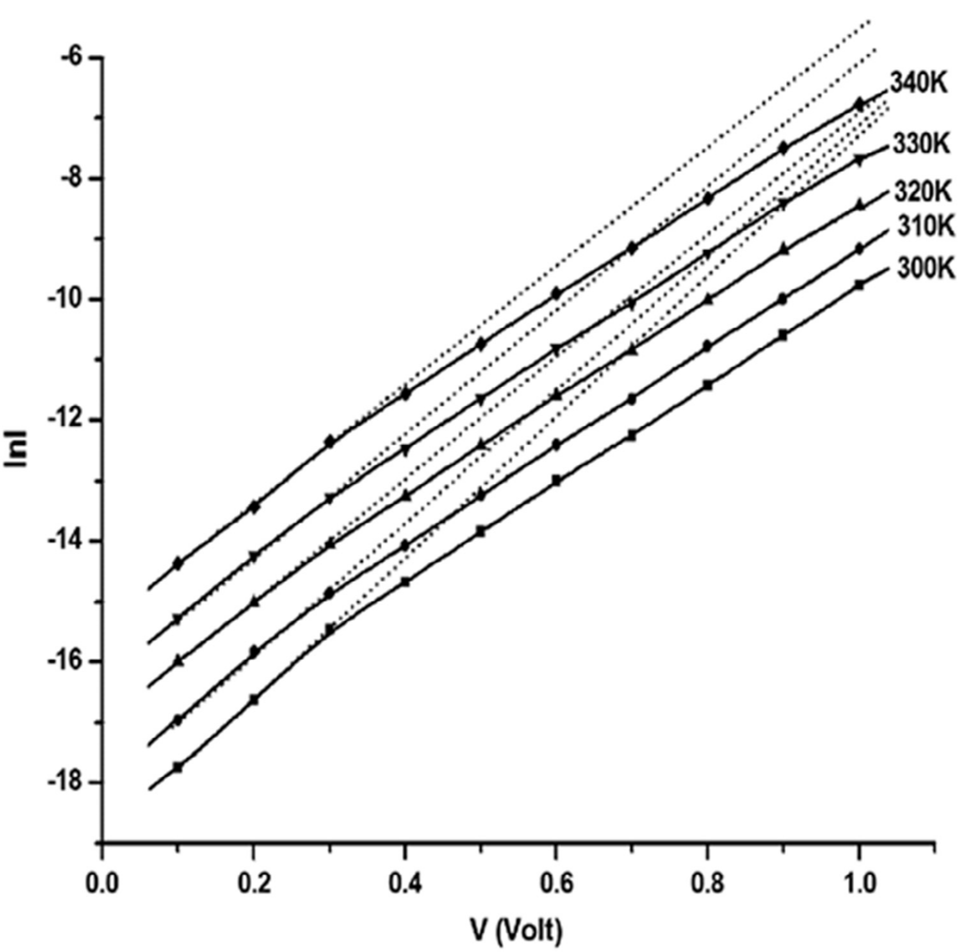

Fig. 7 – lnI vs V plots of a typical (p)Si/(n)Bi_2S_3 heterojunction.

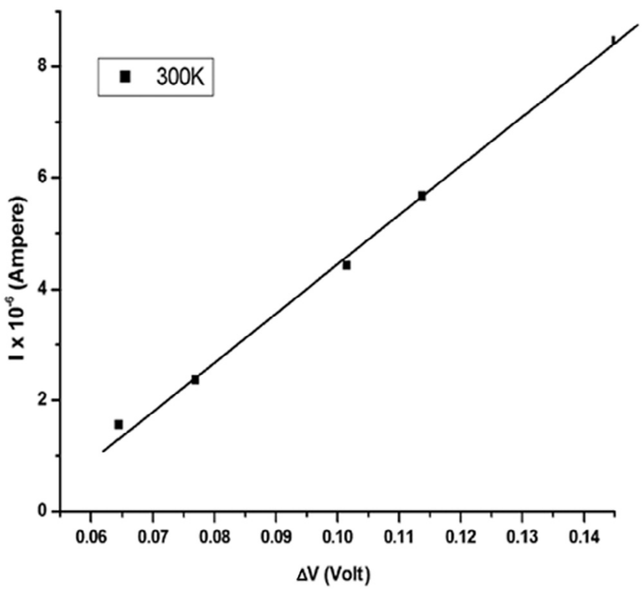

Fig. 8 – Plot of I vs ΔV of a typical (p)Si/(n)Bi_2S_3 heterojunction.

3.5. *Capacitance–voltage characteristics of a (p)Si/(n)Bi_2S_3 junction*

The capacitance–voltage characteristics of (p)Si/(n)Bi_2S_3 junction is measured at 1 KHz frequency under reverse bias condition at room temperature (300 K). Fig. 9 shows C^{-2}–V plot of a typical (p)Si/(n)Bi_2S_3 junction. The built-in potential V_{bi} measured from this plot is found to be 0.69 eV, which is higher than the value obtained from current–voltage characteristics as given in Table 2. This divergence is ascribed to the existence of capacitance at the interfacial layer containing defects [57,58]. Other factors for this divergence are lowering of the barrier height

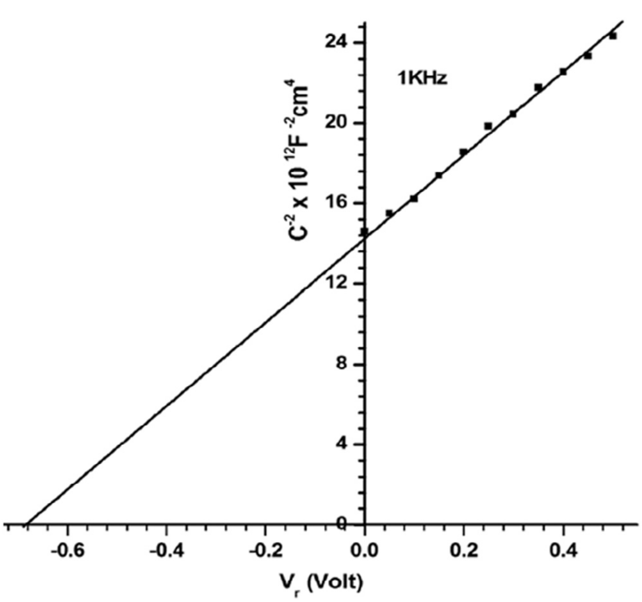

Fig. 9 – C^{-2}–V plot of (p)Si/(n)Bi_2S_3 heterojunction measured at 300 K.

by image force in the I–V characteristics and the barrier height inhomogeneities [59,60].

3.6. *Photovoltaic measurements of (p)Si/(n)Bi_2S_3 heterojunction*

The photovoltaic performance of the (p)Si/(n)Bi_2S_3 junction is investigated under different light intensities. Fig. 10 shows J–V curves for a typical (p)Si/(n)Bi_2S_3 junction under different light intensities, which reveals poor photovoltaic effect of the junctions. Under illumination, electron–hole pairs are created inside the depletion region and are separated by built-in electric field with holes and electrons are drifting to the Si and Bi_2S_3layers respectively. When the device terminals are short-circuited, excess holes in the Si flow through the external circuit to recombine with the excess electrons in the Bi_2S_3 side and this represents the photocurrent. Calculated photovoltaic parameters of the junctions are given in Table 3. The open-circuit voltage and short-circuit current are strongly dependent on the series resistance (R_s) as well as the junction ideality factor (n) as per the known equations [61].

$$I_{SC} = I_0\left[\exp\left(\frac{q(V - IR_S)}{kT}\right) - 1\right] - I \tag{9}$$

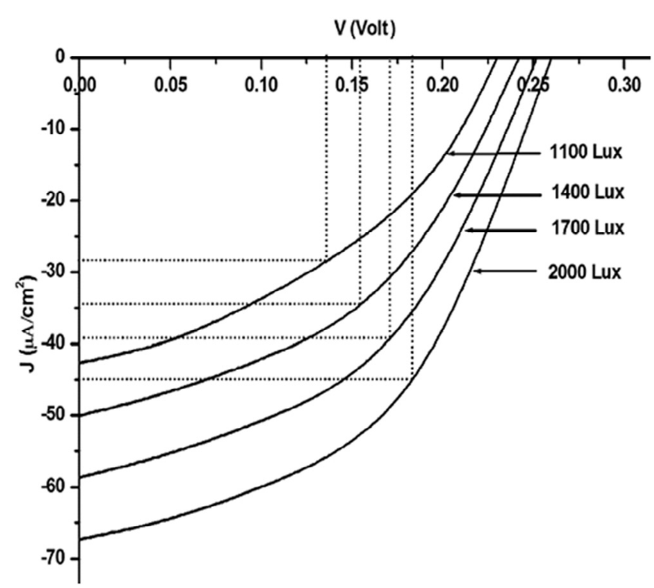

Fig. 10 – J–V plots of a typical (p)Si/(n)Bi_2S_3 junction at different light intensities.

Table 3 – Photovoltaic parameters of a typical (p)Si/(n)Bi_2S_3 heterojunction.

Intensity of light (Lux)	Short-circuit current (J_{sc} μA/cm^2)	Open-circuit voltage V_{oc} (Volt)	Fill factor (FF)	Efficiency (%)
1100	42.623	0.232	0.390	0.385
1400	50.03	0.242	0.436	0.414
1700	58.67	0.252	0.452	0.432
2000	67.31	0.200	0.605	0.447

$$V_{OC} = \frac{nkT}{q} \ln\left(\frac{I_{SC}}{I_o} + 1\right) \tag{10}$$

where, I is the total output current and I_o is the saturation current. The open-circuit voltage (V_{oc}), short-circuit current density (J_{sc}) and fill factor of these junctions are tabulated in Table 3. It is observed that the junction exhibits poor photovoltaic performance with low fill factor and low efficiency. In the polycrystalline films, the grain boundary potential may affect the series resistance and open-circuit voltage of solar cell [62]. Recombination of electron–hole pairs photo-generated takes place at grain boundary and hence the short-circuit current is reduced [63]. Besides, there are many factors responsible for the poor photovoltaic performance, such as presence of interfacial layer and low doping concentration. As the light intensity increases there is increase in excitation and separation of electrons from their atoms, which leads to the creation of more electron–hole pairs. This may be the reason for the increase of photovoltaic performance of the junctions with increasing light intensity.

4. Conclusions

In this paper, we investigated the temperature dependent electrical and photovoltaic properties of (p)Si/(n)Bi_2S_3 heterojunction fabricated by chemical bath deposition (CBD) technique. The rectifying nature of the junction shows the formation of barrier at the interface of the two semiconductors. The ideality factor and series resistance decreases, whereas the potential barrier height increases with increase in temperature. Photovoltaic conversion efficiency of the junction is found low with low value of fill factor due to the presence of the interfacial and barrier height inhomogeneity.

Acknowledgement

We express our gratefulness to the Department of Physics, Manipur University, Manipur, for providing the SEM facilities.

REFERENCES

[1] Novoselova AB, editor. Physical and chemical properties of semiconductors handbook. Moscow: Nauka; 1978. p. 97.
[2] Pari N, Nayak BB, Acharya BS. Thin Solid Films 1995;254:47.
[3] Chapnik IM. Phys Status Solidi 1986;137B:95.
[4] Li Y, Wei F, Ma Y, Zhang H, Gao Z, Dai L, et al. CrystEngComm 2013;15:6611–16.
[5] Bube RH. Photoconductivity in solids. New York: Wiley; 1960.
[6] Mizogushi H, Hosono H, Ueda N, Kawazoe K. J Appl Phys 1995;78:1376.
[7] Martiny JM, Hernandezy JL, Adellyz L, Rodriguezy A, Lopez F. Semicond Sci Technol 1996;11:1740–4.
[8] Song L, Chen C, Zhang S. Power Technol 2011;207:170–4.
[9] Pejova B, Grozdanov I. Mater Chem Phys 2006;99:39.
[10] Killerdar VV, Lokhande CD, Bhosale CH. Thin Solid Films 1996;289:14–16.
[11] Ubale AU. Mater Chem Phys 2010;121:555–60.
[12] Jana A, Bhattacharya C, Sinha S, Datta J. J Solid State Electrochem 2009;13:1339–50.
[13] Ahire RR, Sharma RP. Indian J Eng Mater Sci 2006;13:140–4.
[14] Mane RS, Shankapal BR, Lokhande CD. Mater Res Bull 2000;35:587–601.
[15] Lokhande CD, Ubale AU, Patil PS. Thin Solid Films 1997;302:1–4.
[16] Desai JD, Lokhande CD. Mater Chem Phys 1995;41:98–103.
[17] Lukose J, Pradeep B. Solid State Commun 1991;78:535–8.
[18] Mahmoud S, Sharaf F. Fizika 1996;A5:205–13.
[19] Mageshwari K, Sathyamoorthy R, Sudhagar P, Kang YS. Appl Surf Sci 2011;257:7245–53.
[20] Mageshwari K, Sathyamoorthy R. Vacuum 2012;86:2029–34.
[21] Lokhande CD, Bhosale CH. Bull Electrochem 1990;6:622.
[22] Miller B, Menzes S, Heller A. J Electroanal Chem 1978;94:85–9.
[23] Krishnamoorthy PA, Shivkumar GK. Thin Solid Films 1984;121:151.
[24] Pawar SH, Bhosale PN, Uplane MD, Tamhankar SP. Thin Solid Films 1983;110:165–70.
[25] Pawar SH, Tamhankar SP, Lokhande CD. Mater Chem Phys 1984;11:401–12.
[26] Mahmoud SA. Physica B 2001;301:310–17.
[27] Benramdane N, Latreche M, Tabet H, Boukhalfa M, Kebbab Z, Bouzidi A. Mater Sci Eng B 1999;64:84–7.
[28] Medles M, Benramdane N, Bouzidi A, Nakrela A, Tabet-Derraz H, Kebbab Z, et al. Thin Solid Films 2006;497:58–64.
[29] Wang SY, Du YW. J Cryst Growth 2002;236:627–34.
[30] Wang H, Zhu JJ, Zhu JM, Chen HY. J Phys Chem B 2002;106:3848–54.
[31] Liao XH, Wang H, Zhu JJ, Chen HY. Mater Res Bull 2001;36:2339–46.
[32] Liao XH, Zhu JJ, Chen HY. Mater Sci Eng B 2001;85:85–9.
[33] Shao MW, Mo MS, Cui Y, Chen G, Qian YT. J Cryst Growth 2001;233:799–802.
[34] Zhang W, Yang Z, Huang X, Zhang S, Yu W, Qian Y, et al. Solid State Commun 2001;119:143.
[35] Yu SH, Yang J, Wu YS, Han ZH, Xie Y, Qian YT. Mater Res Bull 1998;33:1661–6.
[36] Yu SH, Shu L, Yang JA, Han ZH, Qian YT, Zhang YH. J Mater Res 1999;14:4157.
[37] Pineda E, Nicho ME, Nair PK, Hu H. Sol Energy 2012;86:1017–22.
[38] Martinez L, Stavrinadis A, Higuchi S, Diedenhofen SL, Bernechea M, Tajimab K, et al. Phys Chem Chem Phys 2013;15:5482–7.
[39] Becerra D, Nair MTS, Nair PK. J Electrochem Soc 2011;158:H741–9.
[40] Moreno-Garcia H, Nair MTS, Nair PK. Thin Solid Films 2011;519:2287–95.
[41] Moreno-García H, Nair MTS, Nair PK. Thin Solid Films 2011;519:7364–8.
[42] Kachari T, Wary G, Rahman A. AIP Conf Proc 2010;1249:202–5.
[43] Bao HF, Cui XQ, Li CM, Gan Y, Zhang J, Guo J. J Phys Chem 2007;C.111:12279–83.
[44] Bessekhouad Y, Robert D, Weber JV. J Photoch Photobio A 2004;163:569–80.
[45] Moreno-García H, Gomez-Daza O, Campos J, Nair MTS, Nair PK. Mater Res Soc Symp Proc 2007;1012:451.
[46] Wang ZJ, Qu SC, Xu Y, Chen YH, Zeng XB, Liu JP, et al. Adv Mater Res 2007;26–28:601–7.
[47] Ladhe RD, Baviskar PK, Tan WW, Zhang JB, Lokhande CD, Sankapal BR. J Phys D Appl Phys 2010;43(1–6):245302.
[48] Rath AK, Bernechea M, Martinez L, Konstantatos G. Adv Mater 2011;23:3712–17.
[49] Hussain A, Begum A, Rahman A. Indian J Phys 2012;86(8):697–701.

[50] Hussain A, Rahman A. Mater Sci Semicon Proc 2013;16:1918–24.
[51] Reddy NNK, Reddy VR. Bull Mater Sci 2012;35(1):53–61.
[52] Sze SM. Physics of semiconductor and devices. 2nd ed. New Delhi: Willy Eastern Ltd.; 1983. p. 126–46.
[53] Rhoderick EH, Williams RH, editors. Metal-semiconductor contacts. Second ed. Oxford: Clarendon Press; 1988.
[54] Werner JH, Ploog K, Queisser HJ. Phys Rev Lett 1986;57:1080–3.
[55] Werner JH, Gutter HH. J Appl Phys 1991;69:1522–33.
[56] Janardhanam V, Lee H-K, Shim K-H, Hong H-B, Lee S-H, Ahn K-S, et al. J Alloy Compd 2010;504:146–50.
[57] Van Zeghbroeck B. Principles of electronic devices. 1996; Electronic Book.
[58] Peta KR, Park B-G, Lee S-T, Kim M-D, Oh J-E, Kim T-G, et al. Thin Solid Films 2013;534:603–8.
[59] Card HC, Rhoderick EH. J Phys D Appl Phys 1971;4:1589–601.
[60] Cakar M, Onganer Y, Turut A. Synth Met 2002;126:213–18.
[61] Wary G, Kachari T, Rahman A. Int J Thermophys 2006;27:332–46.
[62] Chu TL, Chu SS. Solid-State Electron 1995;38:533–49.
[63] Dutta J, Bhattacharyya D, Chaudhuri S, Pal AK. Sol Energ Mat Sol C 1995;36:357–68.